

Tracking of Vehicles across Multiple Radiance and Reflectance Hyperspectral Datasets

Emmett J. Ientilucci^a, Stefania Matteoli^b, and John P. Kerekes^a

^aDigital Imaging and remote Sensing Laboratory, Rochester Institute of Technology,
54 Lomb Memorial Drive, Rochester, NY 14623-5604

^bDepartment of Information Engineering, University of Pisa, via Caruso 16, 56122, Pisa, Italy

ABSTRACT

Tracking of vehicles, in both radiance and reflectance hyperspectral imagery, was analyzed using traditional reflectance domain and forward predicting physics based target detection algorithms. The investigation consisted of locating vehicles in one image followed by locating the same (relocated) vehicles in another image that was collected at a different time. Traditional approaches to hyperspectral target detection involve the application of detection algorithms to atmospherically compensated imagery. Rather than compensate the imagery, a more recent approach uses physical models to generate radiance signature spaces. The signature space is actually a representation of what the target might look like to the sensor as the reflectance propagates through the atmosphere. The model takes into account atmospheric conditions, illumination conditions and target reflectivity. Different collection times have varying atmospheric conditions leading to changes in the sensor-reaching radiance spectrum. A forward predicting physical model, applied in the radiance domain, handles this variation. The data used in this study is a new ground truthed hyperspectral data set, collected with the airborne HyMap sensor, and which is now freely available to the community through the web for evaluation, testing, and algorithm development. Vehicles were relocated across various flight lines. This paper compares vehicle detection results, across these multiple images collected within a short time period, using both the physical model and the traditional atmospheric compensation approach.

Keywords: Target detection, hyperspectral imaging, physics based modeling, target tracking

1. INTRODUCTION

Traditional passive material detection of hyperspectral data is typically performed on atmospherically compensated data where the formulations of the various compensation algorithms, together with all the detector scheme variants, leads to solutions that are very scene and application dependant. Radiance domain processing is an alternative to reflectance domain processing where predictions of the at-sensor reaching radiance are determined. Here too, we see many detection algorithm variants. In an application such as tracking, or material detection across multiple images, it is unclear if there exists any advantage of processing in one domain versus another.

For this study, two recently acquired data sets were evaluated each collected at a different time. For each of the two collects, there exists a calibrated radiance and atmospherically compensated cube. Vehicles were placed in one collect and then moved to a random location in the second collect. Material identification was performed on both collections using radiance and reflectance imagery (i.e., four data cubes). In addition, a couple common detection schemes found in literature were applied to all four cubes.

The end goal in this study is two fold. The first is to apply both radiance domain and reflectance domain processing to multiple data sets with the idea of tracking a common material through out the imagery. Investigation is into whether there is one type of processing chain (reflectance imagery using a GLRT, for example) that is preferred over another. The second goal is to introduce a new freely available hyperspectral data set to the community, where there exists a web site containing ground truth, spectra, and a free service to evaluate detection results from a blind study.

Further Information:

emmett@cis.rit.edu, Tel: 585-475-7778, Fax: 585-475-5988

stefania.matteoli@iet.unipi.it, Tel: +39 050 2217 579 Fax: +39 050 2217 522

kerekes@cis.rit.edu, Tel: 585-475-6996, Fax: 585-475-5988

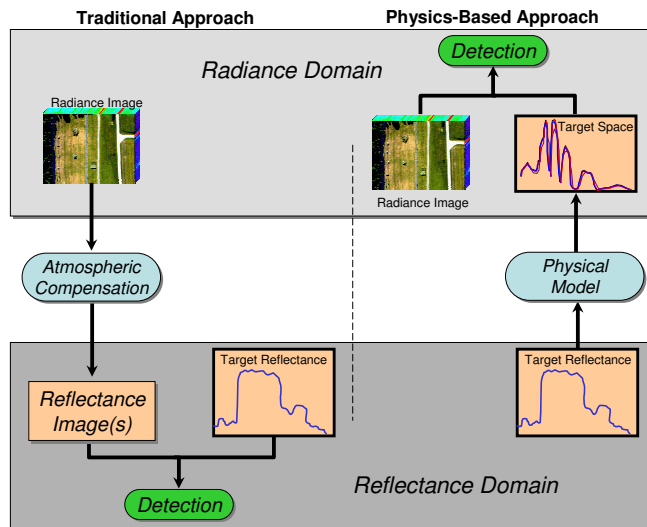


Figure 1. Illustrated are traditional and physics-based approaches to target detection. The traditional approach moves the imagery from the radiance domain to the reflectance domain, where detection is performed. The physics-based approach moves the target reflectance to the radiance domain, where detection is performed.

2. BACKGROUND AND THEORY

2.1 Reflectance Approaches to Material Detection

In a reflectance based approach to material detection one attempts to match a target reflectance signature, either field or laboratory measured, against every pixel in an image in hopes of finding pixels that resemble the target reflectance. Whatever the matching algorithm, or target detector, the end result is typically a single band gray scale image where brightness is usually proportional to the quality of the match. In order to perform this match both the target signature and image data need to be in the same domain. For the case of reflectance material detection, the imagery is typically compensated so as to remove any atmospheric effects. That is, one attempts to remove atmospheric contributions to the sensor-reaching spectra so as to obtain ground-leaving reflectance.

There are many techniques in the literature that attempt to atmospherically compensate imagery and to date, this process of atmospheric compensation is one of the most difficult tasks facing the remote sensing community. At present, no single approach has proven sufficiently simple, accurate, and robust enough to be widely accepted and operationally used. As a result, a number of methods for atmospheric compensation exist that are useful for a particular type of problem or accuracy level. Some estimate surface reflectance while others obtain ground temperature / emissivity information. In general, compensation algorithms can employ field measurements (ground truth) at the time of overflight (e.g., empirical line method (ELM)), in-scene measurements, and / or information from radiation propagation models. For this research, we will be working with surface reflectance in the VIS-NIR and SWIR.

2.2 Radiance Approach to Material Detection

As previously mentioned, atmospheric compensation is often desired prior to a target signature matching process. That is, once the imagery has been compensated, detection algorithms are used to compare image reflectance's to library or measured reflectance's in search of a desired target. This process of searching or matching in a common domain can be seen in Figure 1. Rather than compensate the imagery, an alternative is to estimate what the ground leaving spectral reflectance would look like as seen by the sensor in radiance space.¹ This approach entails modeling the propagation of a reflectance spectrum through the atmosphere up to the sensor.

The advantage this technique has over that of compensated imagery is that target illumination variations, for example, can be integrated into the process through use of a physical model thus making the approach *invariant* to illumination effects. Since we are using a model, we can potentially incorporate any variation in

the reflectance signature such as contamination or adjacency effects. If one wishes to implement variations on an atmospheric parameter, for example, using the *compensation approach*, we would need to generate *multiple* reflectance hypercubes. However, any variation of a sensor-reaching radiance spectrum, using a physical model, simply manifests itself as multiple spectra in a signature or *target space*.

The physics-based model that has been used for this research approach is one derived by Schott.² In simplest form, the spectral radiance reaching an airborne or satellite sensor can be expressed as

$$L_p(\lambda) = \int_{\lambda} \beta_p(\lambda) \left[\left(E'_s(\lambda) \tau_1(\lambda) \cos \theta + F E_d(\lambda) \right) \tau_2(\lambda) \frac{r(\lambda)}{\pi} + L_u(\lambda) \right] d\lambda \quad (1)$$

where $L_p(\lambda)$ is the effective spectral radiance in the p^{th} band in units of $[Wcm^{-2}sr^{-1}\mu m^{-1}]$, $E'_s(\lambda)$ is the exoatmospheric spectral irradiance from the Sun in units of $[Wcm^{-2}\mu m^{-1}]$, $\tau_1(\lambda)$ is the transmission through the atmosphere along the Sun-target path, θ is the angle from the surface normal to the Sun, F is the fraction of the spectral irradiance from the sky ($E_d(\lambda)$), incident on the target (*i.e.*, not blocked by adjacent objects), sometimes called shape factor, $\tau_2(\lambda)$ is the transmission along the target-sensor path, $r(\lambda)$ is the spectral reflectance factor for the target of interest (*i.e.*, $r(\lambda)/\pi$ is the bidirectional reflectance $[sr^{-1}]$), $L_u(\lambda)$ is the spectral path radiance $[Wcm^{-2}sr^{-1}\mu m^{-1}]$, and $\beta_p(\lambda)$ is the normalized spectral response of the p^{th} spectral channel of the sensor under study where

$$\beta_p(\lambda) = \frac{\beta'_p(\lambda)}{\int \beta'_p(\lambda) d\lambda} \quad (2)$$

with $\beta'_p(\lambda)$ being the peak normalized spectral response of the p^{th} channel. We can then use a radiative transfer code such as MODTRAN³ to solve for each of the radiometric terms in Eq. (1) (*i.e.*, $E'_s(\lambda)$, $\tau_1(\lambda)$, $\tau_2(\lambda)$, $E_d(\lambda)$, and $L_u(\lambda)$) given a set of atmospheric and illumination descriptors. Once the terms are solved for, the spectral radiance signature or target vector \mathbf{x} observed by a p -channel sensor can be expressed as

$$\mathbf{x} = [L_1(\lambda), L_2(\lambda), \dots, L_p(\lambda)]^T. \quad (3)$$

2.3 Physically Derived Signature Spaces

A physically derived signature space (PDSS) or target space can be used in any application where an estimate of a sensor-reaching radiance signature is required. For instance, PDSS's have been used for gas detection⁴ and for man-made target detection.⁵ The research presented in this study demonstrates the PDSS approach for the latter application, showing the use of signature spaces (target spaces) for hyperspectral target detection.

The model of Eq. (1) generates a single estimate of the target, as seen by the sensor. In practice, however, a *family* of radiance vectors is usually generated to account for lack of knowledge about the atmospheric, illumination and viewing conditions. This is accomplished by varying the inputs to MODTRAN (and/or the physical model) to span a range of variables or levels. In doing so, a range of potential target spectral vectors spanning a *target space* can be generated from a single target reflectance spectrum. In general, many of the input parameters to MODTRAN are usually known at the time of image acquisition or can be reasonably estimated (*e.g.*, atmospheric and aerosol model, day of year, location, time of day, etc.). For this approach, emphasis is placed on varying MODTRAN parameters that are more likely to be unknown. These include visibility (V), water vapor scale factor (WV) and ground topography (T) or what might be thought of as change in ground elevation. In the case of water vapor scale factor, a physics based atmospheric compensation algorithm can be used to estimate per pixel total column water vapor which can then be converted to an appropriate range of scale factors. In addition to classical MODTRAN input parameters, terms such as shape factor (SF) and target orientation are also varied. These terms, to be discussed, modulate the downwelled and direct solar terms, respectively.

To account for situations where the target is not exposed to the entire hemispherical downwelling radiance (*i.e.*, flux not directly from the Sun but rather scattered from the atmosphere itself) we introduce a scalar term called the shape factor (SF). This term simply reduces the total hemispherical downwelled term to account for the possibility of nearby objects that would block a portion of the sky dome. For example, if the target was flat, horizontal to the Earth's surface, and unobstructed such that the entire hemisphere above the target was sky, the shape factor value would be 1. That is, no attenuation of the total calculated downwelled radiance term.

The target orientation term is really a mechanism to account for illumination effects. For this approach, the solar zenith angle is known (and fixed), because we assume the user has some *a priori* knowledge about when the imagery was collected (*i.e.*, time of day and location). Even if the spectral character of the target, as seen by the sensor through the atmosphere, is modeled correctly in MODTRAN, we may still have issues related to spectral magnitude. This can manifest itself as a time of day variation, target-to-sensor angle or orientation variation, or both. In this research we factor in an additional parameter that allows the user to vary the *orientation* of the target relative to the Sun, in a 2D sense.

This variation in target orientation, or more precisely illumination (IL), is simply a modulation of the direct solar term to account for projected area effects. We implement this as a target rotation angle relative to the zenith angle determined in MODTRAN, for the time of day. If the rotation is zero, then there is no adjustment of the direct term. However, a positive or negative rotation angle implies that we have rotated the target toward or away from the Sun, respectively. The relation for this modulation of the direct term is

$$E_{s_new}(\lambda) = \frac{E_s(\lambda)}{\cos \sigma'} \cos \sigma_{new} \quad (4)$$

where $E_s(\lambda) = E'_s(\lambda) \cos \sigma'$, $\sigma_{new} = \sigma' - \sigma_{rot}$ and σ_{rot} is the user specified angle of rotation. The zenith angle σ' comes from MODTRAN output. It is important to note here that $E_s(\lambda)$ in this notation comes directly from MODTRAN and already has the zenith angle attenuation applied to it. We differentiate this value from $E'_s(\lambda)$ which is the direct solar term without any angular effects. As an example, if the zenith angle was 60 degrees and we specified a rotation angle of $\sigma_{rot} = -10$ degrees, then we would have

$$E_{s_new}(\lambda) = \frac{E_s(\lambda)}{\cos 60} \cos(60 - (-10)) = 0.68E_s(\lambda) \quad (5)$$

which says we have effectively reduced the direct-term illumination onto the target by 32%. Additional information describing these parameters as they apply to target space generation can be found in the literature.⁵

The actual target spaces are then created through a series of MODTRAN runs followed by a set of C-shell UNIX scripts used to parse the MODTRAN output. Since computation time can be burdensome, all the runs are submitted to a workload management system for compute intensive jobs. This management system provides a job queueing mechanism, scheduling policy, priority scheme, and resource management which makes the hundreds of MODTRAN runs, and this approach to signature space creation, possible. Upon completion of the submitted jobs, the MODTRAN output files are parsed so as to obtain the various terms in the sensor-reaching radiance equation. These spectral quantities are then resampled using a user supplied sensor response file. Finally, the resampled quantities are assembled into an ASCII look-up-table (LUT) to be used as input to the physics based model described in Eq. (1).

2.4 Detection Schemes

Matching or detection algorithms can be applied to either the previously mentioned reflectance or radiance imagery. There are many to choose from where some work better than others, depending on application. This is yet another area of remote sensing where it is still unclear as to which algorithms work best in which domain-type imagery. For this research, we will focus on two approaches to detection, one that deals with addressing the geometry of the data (*i.e.*, vector algebra) and another stochastic approach that takes advantage of first and second moments. The algorithm used from the geometric point of view is the generalized likelihood ratio test (GLRT)⁶ which has the form

$$T(x) = \left(\frac{x^T P_B^\perp x}{x^T P_Z^\perp x} \right)^{\frac{1}{2}} \quad (6)$$

where x is a spectral vector from the image and $Z = [T, B]$ is a matrix consisting of all columns of T and B , and P_Y^\perp (for Y equal to B or Z) is the matrix of the projection onto the space orthogonal to the space generated by columns of Y . That is

$$P_Y^\perp = I - Y(Y^T Y)^{-1} Y^T \quad (7)$$

$$= I - Y Y^\dagger \quad (8)$$

Table 1. Summary specification for vehicles to be tracked.

Name	Model	Color	Pixels On Target
V1	Chevy Blazer	Green	1
V2	Toyota T100 Pickup	White/Black Bed	1
V3	Subaru GL Wagon	Red	1

where I is the identity matrix and $Y^\dagger = (Y^T Y)^{-1} Y^T$ is the pseudo-inverse of Y . For this research, the matrix B was obtained by computing basis vectors from the image through use of the singular value decomposition (SVD). For this study, the first 10 components were used to populate the matrix B . The matrix T was obtained by either computing an SVD on the radiance target signature space and keeping the first three components, computing a mean vector of the radiance target space, or by simply using a single vector, such as a reflectance spectrum, in the reflectance domain experiments.

The second detector that was used is called the adaptive coherence estimator (ACE)⁷ and takes on the form

$$T(x) = \frac{x^t \Sigma_b^{-1} T (T^T \Sigma_b^{-1} T) T^t \Sigma_b^{-1} x}{x^t \Sigma_b^{-1} x} \quad (9)$$

where we have the inverse covariance of the background data as Σ_b^{-1} . The matrix T is either a single library reflectance signature, the first three components from an SVD of the radiance target space, or a mean vector of the target space.

2.5 Free Hyperspectral Data Set(s)

The hyperspectral data used in this research was acquired by the airborne HyMap sensor⁸ over Cook City, Montana, on July 4th, 2006. The image consists of 126 spectral channels in the VNIR-SWIR with dimensions of 280 x 800 pixels and a ground sampling distance (GSD) of about 3 meters. A true-color representation of the area can be seen in Figure 2.

During acquisition, different types of targets were present in the scene, some fabric panels and some vehicles. Specifically, the vehicles that were tracked can be seen in Figure 4. These were a Chevy Blazer (V1), Toyota T100 (V2) and a Subaru GL wagon (V3) (see Table 1). Vehicle V2 was actually composed of two spectra, one measured from the bed liner and one representing the roof and hood. The first airborne image was collected at 15:20 UCT on July 4th, 2006. Before the second flyover, some 22 minutes later at 15:42 UCT, all three vehicles were moved to different locations throughout the town. Because of the 3.939 km sensor altitude and given GSD (about 3 meters) there is only one mixed pixel on target, thus making the detection challenging, especially in such a cluttered environment. Spectral library reflectance measurements of the targets were available along with ground truth maps in the form of ENVI region of interest (ROI) maps.

An atmospherically compensated reflectance image was provided with the data set. This was obtained by processing the radiance image with an algorithm in the HyCorr[®] software package (HyVista Co.)⁹ designed specifically for HyMap image correction. This image, together with available spectral library measurements, was used to perform target detection in reflectance domain. Detection was also performed on calibrated radiance data, which was also provided.

The data set used in this study is free and can be downloaded at <http://dirtsapps.cis.rit.edu/blindtest>. It is part of a larger project to provide a standard hyperspectral data set to the remote sensing community.¹⁰ Additionally, the project will score the ability of target finding algorithms used on the data set provided. There exists a self-test data set which is fully ground truthed and a blind-test data set where target locations are unknown to the user, but scored upon uploading detection results to the web site. These services are provided for free and after registering, anyone can access the project's data and evaluation services.



Figure 2. Color image of Cooke City, Montana collected with the HyMap hyperspectral sensor.



Figure 3. Zoomed in section of Cooke City, Montana showing location of vehicles in the self-test imagery. The truth mask for each vehicle shows 8 guard pixels around a *single* mixed vehicle pixel.(color images in electronic version of manuscript)



Figure 4. Vehicles to be tracked in the hyperspectral imagery.

Table 2. Data, algorithms, domain, and targets to be evaluated.

Domain	Detection Algorithm	Data Set	Targets
Reflectance	GLRT, ACE	Self-Test, Blind-Test	V1, V2, V3
Radiance	GLRT, ACE	Self-Test, Blind-Test	V1, V2, V3

Table 3. False alarm results using the *self-test* imagery for both the reflectance and radiance domains.

	REFLECTANCE			RADIANCE			
	V1	V2	V3	V1	V2	V3	
				GLRT-Sub3	14	29285	13976
GLRT	212	92248	15521	GLRT-Mean	12749	19180	32337
ACE	49	36617	687	ACE-Sub3	54	17687	930
				ACE-Mean	7541	35346	47813

3. RESULTS

3.1 False Alarms (FA)

The combinatorics associated with this study can be seen in Table 2. For each domain (i.e., reflectance or radiance), we locate vehicles V1, V2 and V3 in both the self- and blind-test data sets using the GLRT and ACE detectors.

The first data set to evaluate was the self-test imagery, as seen in Figure 3. The GLRT and ACE algorithms were applied to both the radiance and reflectance data, as mentioned in Section 2.4. Since there is a single mixed pixel to be found, we simply counted the total number of false alarms before actually detecting the target. This *running count* of false alarms can be seen in Table 3. The notation associated with these false alarms from the radiance domain evaluation is as follows; *Sub3* refers to the fact that an SVD was performed on the target space and the first three vectors were used in the detector (as explain in Section 2.4). *Mean* refers to the fact that a mean radiance vector was computed from the target space and used in the detector.

In the blind-test imagery, all three vehicles were moved to other locations throughout the city, as described in Section 2.5. The same set of detection algorithms and domain processing was applied to this data set as well. The running count of false alarms for this data set can be seen in Table 4 with the same labeling scheme as that of Table 3.

3.2 FA Visualization

Attempting to draw conclusions about which domain might be better to process algorithms in or which detector performed best is fairly difficult if one simply reviews the false alarm numbers found in Tables 3 and 4. This method of comparing raw numbers is not very intuitive. To address this, a series of plots were made to visually assess the entire trade space, all at once. The plots were made in terms of a specific data set (i.e., self- or blind-test) and can be seen in Figures 5 and 6.

These plots were created by first normalizing the total number of false alarms by the total number of pixels in the image (i.e., 224000 pixels). This produces a false alarm rate (FAR) value from zero to one, where *small* values are desirable. We then compute 1-FAR to obtain scores where large values are desirable. This means that

Table 4. False alarm results using the *blind-test* imagery for both the reflectance and radiance domains.

	REFLECTANCE			RADIANCE			
	V1	V2	V3	V1	V2	V3	
				GLRT-Sub3	5339	12617	49081
GLRT	32905	63364	22593	GLRT-Mean	40769	48490	34571
ACE	1641	17990	3499	ACE-Sub3	795	37756	1131
				ACE-Mean	86407	24532	7320

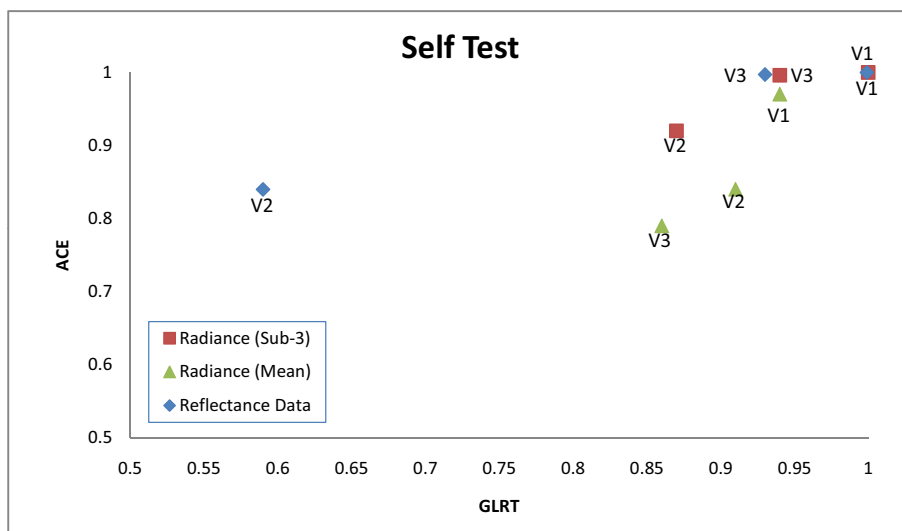


Figure 5. Plot comparing detection algorithm, domain, and target type for the self-test imagery. The reflectance spectrum used was measured at the site, which was used in either reflectance processing or to build a target space for radiance domain processing.(color images in electronic version of manuscript)

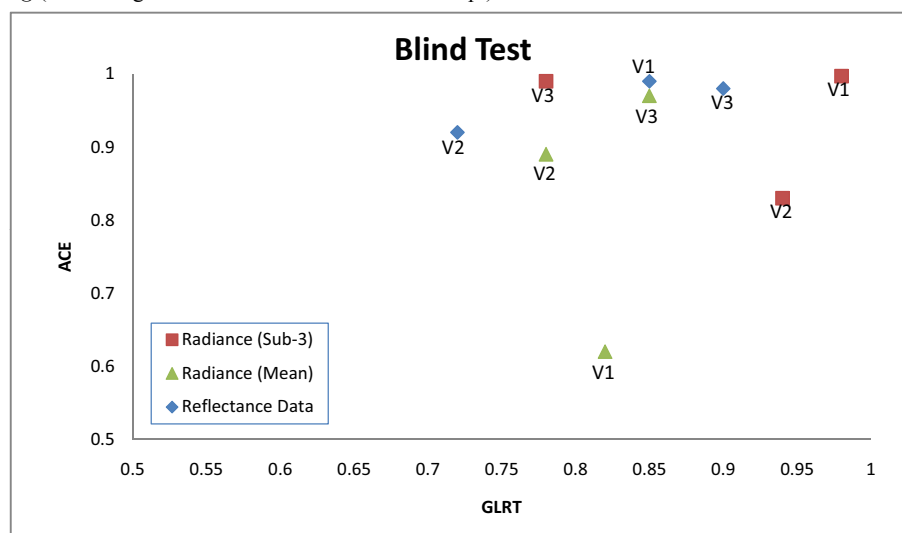


Figure 6. Plot comparing detection algorithm, domain, and target type for the blind-test imagery. The reflectance spectrum used was measured at the site, which was used in either reflectance processing or to build a target space for radiance domain processing.

the best detection scores (i.e., fewest false alarms for a single vehicle target pixel) are found in the upper right hand corner of Figures 5 and 6. The interpretation of such results is addressed in Section 4.

Another experiment was performed in which the spectrum of the vehicle target from the self-test image was used to locate the same target in the blind-test imagery. Though the (large number of) raw false alarms are not shown here, the visualization of such false alarms can be seen in Figure 7 for both the radiance and reflectance domains.

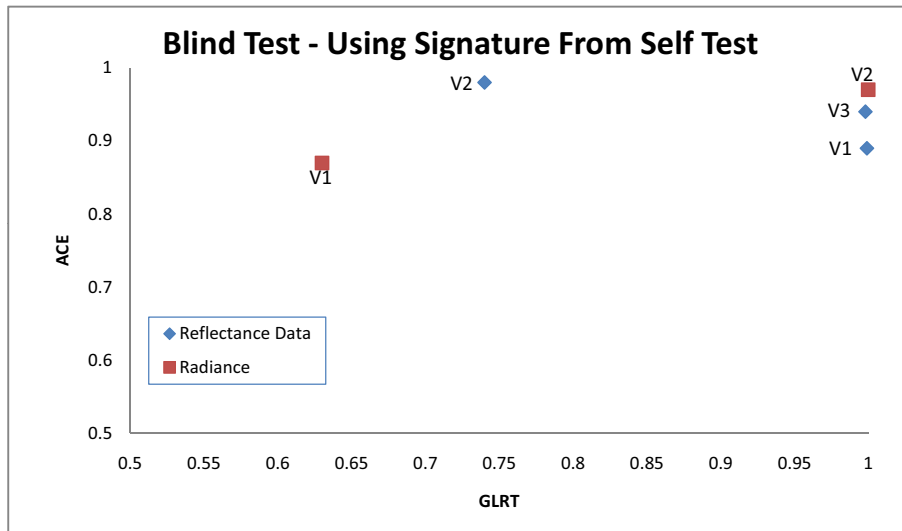


Figure 7. Plot comparing detection algorithm, domain, and target type for the blind-test imagery where the vehicle target spectrum from the self-test image was used to locate the same target in the blind-test imagery.

4. DISCUSSION

The goal of this study was to see if there is any advantage to processing in the radiance domain over the reflectance domain, in a given application such as target tracking. We will address this question by evaluating Figures 5, 6 and 7. When looking at the self-test image results of Figure 5 we really do not see an obvious preference for domain, other than the radiance domain producing better scores for V2. In terms of target difficulty, we see that V2 is certainly the more difficult target to detect. This is due to the fact that V2 is actually made of an *average* of two spectra, one for the bed liner and one representative of the roof and hood. Vehicle one is the easiest to detect. The GLRT has a hard time finding V2 but both algorithms performed about the same.

The blind-test results of Figure 6 shows a much larger detection spread overall, hence a very large number of false alarms, as can be seen in Table 4. In terms of domain preference, the radiance domain has some of the highest scores associated with the easiest target V1. However, if we simply evaluate the domain preference using each detector separately, we see that the radiance domain is preferred using the GLRT while there is no preference when analyzing scores from the ACE algorithm alone. Here again, we see that target V1 is the easiest to detect followed by targets V3 and V2. From a detector point of view, aside from performing poorly on the easiest target V1, the ACE algorithm generally outperforms the GLRT as can be seen by the smaller spread in scores.

In the last experiment, where the reflectance or radiance target signature from the self test data was used in the detection algorithm to find the same target in the blind test data, we see mixed results. For reference, these results were shown in Figure 4. If the originating pixel was truly a full pixel, than the only difference between similar target pixels in the two images should be atmospheric, adjacency, etc. However, the pixels under test were *mixed* with background so there is an added uncertainty in the pixel spectrum due to differences in mixing from scene to scene. In terms of a domain preference, we can see from Figure 4 that there is a slight preference for processing in the reflectance domain. When processing the radiance data, the vehicle V3, doesn't even show up in the plot. Once again, the ACE algorithm seems to outperform the GLRT in this experiment. Though V1 is the easiest target to find, in general, the GLRT surprisingly scores it very low, along with the more difficult target V2.

4.1 Overall Comments

The take away in this study was to analyze any potential differences in reflectance versus radiance domain processing. In general, it was found that there was a slight preference towards processing in the radiance

domain. However, the complexity of the data set, along with various sources of error (leading to large numbers of false alarms) overshadows this conclusion leading one to believe that, for this data set, there is no advantage to processing in one domain versus the other.

The challenge is really in the fact that each target consists of a single mixed pixel in a highly cluttered background. Furthermore, the mixing for each target changed once it was moved in the blind test imagery, thus altering the spectra. This made vehicle tracking even more challenging. However, it should be noted that at the blind test web site, which is where this data resides, (i.e., <http://dirsapps.cis.rit.edu/blindtest>), there exists algorithms that have performed exceptionally well on both reflectance and radiance data sets. A repeat of this experiment would involve use of these algorithms, some of which contain methods for, target-like removal or data cleaning, preprocessing, and / or dimensionality reduction. Moreover, a global approach to background estimation (either via SVD or via covariance estimation) was used which, in such a challenging cluttered scenario with a lot of “confusers”, can lead to many false alarms. Finally, it is noted that a much larger study was performed using this data set by Matteoli, *et. al.*¹¹ which addressed some of the weak links in the image chain specifically pertinent to the data set. This study addressed calibration, atmospheric uncertainty, variability in measured reflectance spectra as well as the application of a much larger database of detection algorithms in a variety of configurations.

5. CONCLUSIONS

This study focused on tracking a set of vehicles from one hyperspectral image to another, where the time difference between collections was on the order of minutes. In doing so, the issue of domain preference was addressed. That is, was there any advantage to processing in one domain relative to the other. No real preference was found, though further investigation is required. Moreover, the results presented here might be deemed inconclusive due to the large number of false alarms seen and the overall complexity of the data. Large instances of false alarms were due to a host of factors including standard use of detectors on a very challenging, cluttered, single mixed pixel detection problem. Overall, from this particular study and once again, it is still unclear as to which detector performs best in which domain for a particular target, which comes as no surprise since this is still an issue for the remote sensing community at large. However, more advanced detection algorithms have performed better on this data eluding to the fact that these should be taken into account in future studies.

Lastly, this research tested and evaluated a new (freely) available hyperspectral data set for community use. The previously mention web address enables one to download reflectance, radiance, and ground truth information. Additionally, the user can upload detection scores, using his/her own detection algorithm on the “blind-test” data set, for evaluation and ranking for free of charge.

REFERENCES

1. G. Healey and D. Slater, “Models and methods for automated material identification in hyperspectral imagery acquired under unknown illumination and atmospheric conditions,” *IEEE Trans. Geosci. Rem. Sens.* **37**, pp. 2706–2717, November 1999.
2. J. Schott, *Remote Sensing: The Imaging Chain Approach*, Oxford University Press, New York, 1997.
3. A. Berk, L. Bernstein, and D. Robertson, “MODTRAN: A moderate resolution model for LOWTRAN 7,” Technical Report **GL-TR-89-0122**, Air Force Geophysics Laboratory, Hanscom AFB, MA, 1988.
4. D. Messinger, C. Salvaggio, and N. Sinisgalli, “Detection of gaseous effluents from airborne hyperspectral imagery using physics-based signature predictions,” *Int. J. High Speed Electron. Syst.* **17**, pp. 801–812, December 2007.
5. E. Ientilucci and J. Schott, “Target detection in a structured background environment using an infeasibility metric in an invariant space,” in *Proc. SPIE*, **5806**, pp. 491–502, April 2005.
6. L. Scharf and B. Friedlander, “Matched subspace detectors,” *IEEE Transactions on Signal Processing* **42**, pp. 2146–2157, August 1994.
7. S. Kraut and L. Scharf, “The CFAR adaptive subspace detector is a scale-invariant GLRT,” *IEEE Trans. Signal Process.* **47**(9), pp. 2538–2541, 1999.

8. T. Cocks, R. Jenssen, A. Stewart, I. Wilson, and T. Shields, "The hymap airborne hyperspectral sensor: the system, calibration and performance," in *EARSEL Workshop on Imaging Spectroscopy*, October 1998. HyMap Sensor.
9. HyVista Corporation, Sydney, *HyMap data products*, December 2000.
10. D. Snyder, J. Kerekes, I. Fairweather, R. Crabtree, J. Shive, and S. Hager, "Development of a web-based application to evaluate target finding algorithms," in *Proc. IEEE International Geoscience and remote Sensing Symposium, IGARRS*, **2**, pp. 915–918, (Boston, MA), 2008.
11. S. Matteoli, E. Ientilucci, and J. Kerekes, "Comparison of radiative transfer in physics-based models for an improved understanding of empirical hyperspectral data," in *submitted to IEEE GRSS Workshop on Hyperspectral Image and Signal Processing-evolution in remote sensing, IEEE Whispers-09*, (Grenoble, France), August 2009.